Structural and dynamical properties of Bridgman-grown CdSe[subscript x]Te[subscript 1–x] (0<x≤0.35) ternary alloys

Structural and dynamical properties of Bridgman-grown $CdSe_xTe_{1-x}$ ($0<x\leqslant 0.35$) ternary alloys

Devki N. Talwar*
Department of Physics, Indiana University of Pennsylvania, 975 Oakland Avenue, 56 Weyandt Hall, Indiana, Pennsylvania 15705-1087, USA

Zhe Chuan Feng†
Institute of Photonics and Optoelectronics, Department of Electrical Engineering, and Center for Emerging Material and Advanced Devices, National Taiwan University, Taipei 106-17, Taiwan, Republic of China

Jyh-Fu Lee
National Synchrotron Radiation Research Center, Hsinchu 300-76, Taiwan, Republic of China

P. Becla
Department of Materials Science and Engineering, Massachusetts Institute of Technology, Cambridge, Massachusetts 02139, USA
(Received 15 August 2012; revised manuscript received 20 November 2012; published 29 April 2013)

Measurements of the Raman scattering and extended x-ray-absorption fine-structure (EXAFS) spectroscopy are reported on a series of Bridgman-grown zinc-blende $CdTe_{1-x}Se_x$ ($0.35 \geqslant x > 0.05$) ternary alloys to empathize their lattice dynamical and structural properties. Low-temperature Raman spectra have revealed the classic CdTe-like (TO_1, LO_1) and CdSe-like (TO_2, LO_2) pairs of optical phonons. The composition-dependent peak positions of the LO_2 modes exhibited shifts towards the higher-energy side, while those of the LO_1 phonon frequencies have unveiled the slight redshifts. Detailed analyses of EXAFS data by using the first-principles bond orbital model have enabled us to estimate both the lattice relaxations and nearest-neighbor radial force constants around the Se/Te atoms in the CdTe/CdSe matrix. These results are methodically integrated in the "average t-matrix" formalism within the Green's-function theory for defining the impurity perturbations to comprehend the composition-dependent optical phonons in $CdTe_{1-x}Se_x$ alloys. Based on our comprehensive calculations of impurity modes in the low-composition regime $x \to 0$, we have assigned the weak phonon feature observed near $\sim$175 cm^{-1} in the low-temperature infrared reflectivity spectroscopy study to a Se_{Te} localized vibrational mode.

DOI: 10.1103/PhysRevB.87.165208 PACS number(s): 78.20.Bh, 78.20.Ek, 78.40.Fy

I. INTRODUCTION

Cd-based compound semiconductors with high optical absorption coefficients ($>5 \times 10^5$/cm) and direct band gaps (1.474–2.5 eV) are apposite for engineering integrated microelectronic, sensor, spintronic, photonic, photovoltaic, piezoelectric, and optoelectronic devices.[1–10] Unlike, most II-VI materials, the Cd chalcogenides (CdS, CdSe, and CdTe) exhibit either in the zinc-blende (zb) and wurtzite (wz) crystal structures or in mixed zb/wz phases with varied degrees of ionic/covalent bonding. Earlier use of II-VI compounds[11–20] for the fruition of blue-green light-emitting diodes (LEDs) was hampered by the nonavailability of good-quality crystals and difficulties of managing doping.[21–32] Recent progress in epitaxial techniques has offered preparation of high-quality epilayers and heterostructures on convenient and nearly lattice-matched III-V substrates. Depending upon the growth conditions, it is possible to stabilize one of the two crystal structures either by strain, choosing proper substrates and/or buffer layers, or by controlling the growth temperatures.[1–10] Thin CdS or CdSe epilayers are now grown in the zb phase which does not exhibit the lowest-energy configuration in the bulk.[33]

Despite technological significance of II-VI materials, the prevailing information on their fundamental properties is either sparse or contradictory.[34–37] For instance, while the phonon dispersions of zb CdTe are known from the inelastic neutron-scattering spectroscopy,[37] no such study exists for CdSe and CdS. Earlier, Deligoz *et al.*[34] performed *ab initio* calculations of the elastic, electronic, and lattice dynamical properties of zb Cd chalcogenides; no comparison was made, however, with the experimental data of CdTe[37] to ascertain the accuracy of their simulated values of phonons. A recent study of thermal properties using the full-potential linearized augmented plane-wave method[36] within the density functional theory has provided contradictory results of both the Debye temperature Θ_D and the thermal expansion coefficient α for CdTe.[38]

For ternary compounds, although extensive studies are available[39–52] on the structural and vibrational properties of II-II-VI materials (e.g., CdZnTe, HgZnTe, etc.), there exist limited measurements, however, on the lattice dynamics of alternative II-VI-VI compounds (e.g., CdTeSe, CdSTe, etc.). Earlier IR reflectivity experiments[40,41] in mixed $CdTe_{1-x}Se_x$ alloys with zb structure for $x < 0.35$ and wz structure for $x > 0.5$ suggested the possibility of two-phonon-mode behavior. Other IR studies for $x < 0.35$ performed on the zb $CdTe_{1-x}Se_x$ crystals[43,52] have revealed two major phonons and insinuated a third unresolved feature near $\sim$175 cm^{-1}. Following Verleur and Barker,[53] the origin of an unexpected phonon feature in $CdTe_{1-x}Se_x$ was interpreted[43] in terms of the nonrandom substitutions of the negative ions to cluster around the positive ions. Such a clustering, which tends to make the small regions in ternary alloys either CdTe rich or CdSe rich, was believed to have characteristic effects on the optical phonons as they are strongly dependent upon the Cd-Se, Cd-Te nearest-neighbor bond lengths/force constants. In the low-composition regime

of $CdTe_{1-x}Se_x$, i.e., $x \to 0$, it is likely that the light Se atoms in the CdTe matrix may cause the $\vec{q} \to 0$ conservation rule to relax. Thus, relating the observed unresolved phonon feature near $\sim$175 cm^{-1} [just above the maximum phonon frequency ω_m (170 cm^{-1}) of CdTe] to the localized vibrational mode (LVM) of Se_{Te} in CdTe cannot be completely ruled out; its justification would require, however, realistic lattice dynamical simulations.

The purpose of this paper is to undertake a comprehensive investigation elucidating both the structural and lattice dynamical characteristics of II-VI-VI alloys, especially the composition-dependent variations of the bond lengths in $CdTe_{1-x}Se_x$, and to reexamine its impact on the phonon-mode behaviors (cf. Secs. II A–II C). Low-temperature Raman scattering spectra reported in Sec. II B on the Bridgman-grown zb $CdTe_{1-x}Se_x$ crystals (cf. Sec. II A) are compared with the IR reflectivity data.[52] The extended x-ray-absorption fine-structure (EXAFS) measurements on the same material samples are regarded as imperative in mapping the local atomic structures (cf. Sec. II C). A simple but *first-principles* bond orbital model[54–56] (BOM) used earlier in estimating the structural relaxation is found to be crucial for extorting Cd-Se and Cd-Te bond lengths/strengths in $CdTe_{1-x}Se_x$. This information is meticulously incorporated in the "average t-matrix" (ATM) formalism (cf. Sec. III) using Green's-function theory[57–59] in defining the perturbations for comprehending the composition-dependent optical phonon-mode behaviors (cf. Sec. IV). In simulating self-energy terms, the necessary Green's-function matrix elements of CdTe and zb CdSe are calculated numerically by assimilating phonons from a realistic lattice dynamical rigid-ion model (RIM).[60] The observed impurity modes for the limiting values of x in $CdTe_{1-x}Se_x$ are well described by the ATM–Green's-function methodology.[57,58] Theoretical results of lattice dynamics for the binary and ternary Cd chalcogenides are compared and discussed with the existing experimental/first-principles data,[37,61] with concluding remarks presented in Sec. V.

II. EXPERIMENT

A. Sample preparation

The single-crystal $CdTe_{1-x}Se_x$ samples ($x = 0.05$, 0.15, 0.25, 0.35) considered in the present Raman scattering and XAFS measurements were grown using the Bridgman technique at the Massachusetts Institute of Technology by reacting the 99.9999% pure elemental constituents at approximately 1150 °C in the evacuated sealed quartz tubes. The composition values x were calculated from the mass densities. The precast alloys were regrown at a rate of 0.8–1 mm/h using the directional solidification method in a Bridgman-Stockbarger-type crystal-growth furnace adiabatic zone with a temperature gradient of about $\sim$15 °C/cm. The resulting boules were cut into 1–2-mm-thick slices perpendicular to the growth direction and annealed at 650 °C in a Se atmosphere. Sample crystallinity and orientation were characterized by x-ray data and metallographic etching. All material samples were lapped, polished, etched in a bromine-methanol solution, and found to exhibit in the zb crystal structure.

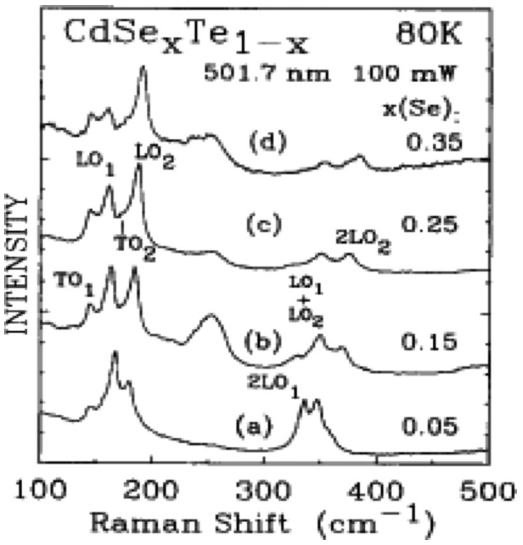

FIG. 1. Raman spectra recorded at 80 K and excited by 501.7 nm on bulk $CdSe_xTe_{1-x}$ samples grown by the Bridgman technique with different x values: (a) 0.05, (b) 0.15, (c) 0.25, and (d) 0.35.

B. Raman scattering spectra

An earlier room-temperature Raman study that we know of on $CdTe_{1-x}Se_x$ excited at 1.06 μm by a YAG:Nd laser come from Plotnichenko *et al.*[42] In Fig. 1, we have displayed our composition-dependent low-temperature (80 K) Raman scattering spectra for four of the $CdTe_{1-x}Se_x$ alloy samples (cf. Sec. II A). An argon-ion (Ar^+) laser source operating at visible wavelengths (501.7 nm) was used to excite the vibrational spectra over the 100–500 cm^{-1} frequency range. This energy region covered both the first- and second-order phonon features. It is well known that for the zb material samples only the longitudinal optical (LO) phonons in Raman spectroscopy are allowed due to selection rules in the (100) backscattering geometry. A few TO modes seen in Fig. 1 are attributed to the relaxation of the $\vec{q}$ conservation law in the scattering process due to alloy disordering and/or by a slight deviation from the true backscattering geometry. Raman spectra in the energy range of 140 and 200 cm^{-1} has revealed CdTe-like and CdSe-like transverse optical (TO) and LO phonons, labeled TO_1, TO_2, LO_1, and LO_2, respectively. Even in a sample with the lowest value of $x = 0.05$ [see Fig. 1, curve (a)], the CdTe-like LO_1, TO_1 and CdSe-like LO_2, TO_2 (very weak) modes are distinguishable; the LO_2 mode appears as a shoulder at the high-energy side of the LO_1. As x increases to 0.15, the LO_1 and LO_2 modes become well separated [see Fig. 1, curve (b)]. For $0.35 \geqslant x \geqslant 0.15$, however, the intensity of the LO_2 line increases and LO_1 decreases, while TO_2 decreases (hardly visible) and TO_1 increases, but only slightly [see Fig. 1, curves (c) and (d)]. The observed vibrational features between 300 and 400 cm^{-1} in Fig. 1 are due to the second-order LO phonons, i.e., the combinations of LO_1 and LO_2, $2LO_1$, $LO_1 + LO_2$, and $2LO_2$. In compound semiconductors the strength of higher-order phonons is generally sensitive to the degree of crystalline perfection. As x increases, the intensities of second-order LO phonon features relative to the first-order peaks decrease, indicating an increased disorder in the material samples. Although we are unable to identify the origin of a

broad feature near ∼250 cm^{-1} [see Fig. 1, curves (b)–(d)], it is probably related either to the disorder or to the defects.

In $CdTe_{1-x}Se_x$ the comparison of Raman scattering data with the existing IR reflectivity spectra[43,52] has undoubtedly revealed two major phonon features in the 140–200 cm^{-1} energy range. For ternary alloys, one must note that while the IR reflectivity spectra in the long-wavelength region are primarily modulated by the TO phonons, these modes in the Raman scattering spectroscopy are either forbidden or hardly discernible. Therefore, for $x \geqslant 0.05$ it is the IR reflectivity[43,52] that provided hints of the CdSe-like TO-phonon splitting near ∼180 cm^{-1} into an additional weak mode, appearing on the lower-energy side (∼175 cm^{-1}), possibly originating either as an alloy disorder or as a LVM of Se_{Te} in CdTe. Earlier, Perkowitz *et al.*[43] used the formalism of Verleur and Barker[53] and interpreted the unexpected mode in $CdTe_{1-x}Se_x$ instigating from the nonrandom substitutions of the negative ions clustering around the positive ions. More recently,[52] the weak phonon feature ∼175 cm^{-1} was contemplated as a LVM of Se_{Te} in CdTe while explicating the observed two-phonon-mode behavior in terms of a modified random-element-isodisplacement (MREI) model. Based on the impurity mode calculations using an ATM–Green's-function theory, we will reaffirm the origin of the observed mode near ∼175 cm^{-1} as a Se_{Te} LVM.

C. X-ray absorption fine-structure spectra

To map the local structures around selected elements in a material system[44–50] XAFS spectroscopy is regarded as one of the most powerful tools. For $CdTe_{1-x}Se_x$ samples with different compositions x, we collected room-temperature XAFS data at the Se K edge (12,658 eV) in x-ray fluorescence (XRF) yield mode at beam line 17-C at the National Synchrotron Radiation Research Center (NSRRC) in Hsinchu, Taiwan. The broadband x-ray spectrum from synchrotron was directed into a double-crystal monochromator (DCM). After minimizing the higher x-ray harmonics by detuning the DCM, a monochromatic x-ray of energy E emerged with a relative bandwidth of about ∼10^{-4} eV. The photon energies were calibrated within an accuracy of ∼0.1 eV using the known Se K-edge peak of CdSe. The beam of incident x-ray photon flux I_o was monitored simultaneously by a Ni-mesh located after the exit slit of the DCM. X-ray photons were incident at an angle of 45° with respect to the sample normal. A microchannel plate (MCP) detector composed of a dual set of MCPs with an electrically isolated grid mounted in the front was used in recording the XRF spectra. For XRF yield detection the grid was set to a voltage of 100 V, while the front and back of the MCPs were set at −2000 and −200 V, respectively. The grid bias ensured that no positive ions were perceived while the MCP bias was maintained to ensure that no electrons were detected. The MCP detector was located nearly 2 cm from the sample and was oriented parallel to the sample surface. A second detector placed behind the sample with thickness d provided transmitted synchrotron radiation (SR) intensity I with absorption coefficient $\mu(E)$ obeying Beer's law, i.e., $I = I_o e^{-\mu(E)d}$.

In Fig. 2(a), we have displayed the SR-XAFS spectra for the Se K-edge absorption coefficient versus photon energy E for four of the $CdTe_{1-x}Se_x$ samples with different compositions. Subtracting the smooth "bare-atom" background $\mu_o(E)$ that fitted the preedge region and dividing it with "edge step"

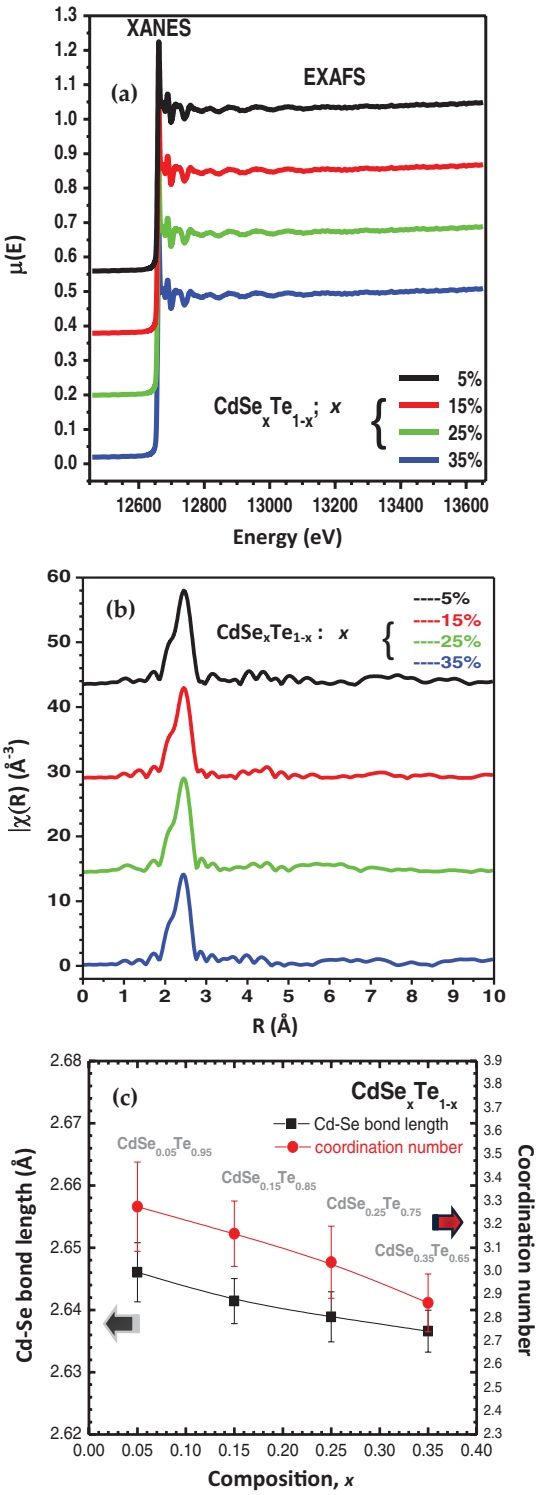

FIG. 2. (Color online) (a) Se K-edge absorption coefficient of Bridgman-grown $CdSe_xTe_{1-x}$ samples of different compositions x (0.05, 0.15, 0.25, and 0.35) as a function of photon energy (see text). (b) Fourier-transformed R-space results of the Se K edge for four $CdSe_xTe_{1-x}$ samples (see text and Table I). (c) Se-Cd bond length and coordination number for four $CdSe_xTe_{1-x}$ samples (see text).

TABLE I. EXAFS results for $CdTe_{1-x}Se_x$ ternary alloys ($x = 0.05$–0.35). X-ray diffraction data of the average bond length (Ref. 67) are also reported for ternary alloys.

x	Coordination number N[a]	Mean square displacement $\Delta\sigma^2$[b]	Binding energy E_o	Experimental EXAFS d[a]	Experimental x-ray d[b]
0					2.782
0.05	3.276	0.00517	1.4530	2.64606	
0.15	3.160	0.00519	2.39832	2.64140	
0.20					2.767
0.25	3.038	0.00495	1.75052	2.63890	
0.30					2.754
0.35	3.864	0.00476	2.25982	2.63661	
0.36					2.737
0.50					2.716
0.60					2.707

[a]Our EXAFS data.
[b]Reference 67.

$\Delta\mu_o(E_o)$, one can extrapolate the simple curve to the edge to give oscillations normalized to one absorption event. The XAFS data shown in Fig. 2(a) consisted of two regimes: (a) x-ray absorption near-edge structure (XANES) and (b) EXAFS. Standard procedures[50] are followed for extracting the bond length and coordination number from the EXAFS data. The XANES region, which started slightly before the absorption edge and extended about ~30 eV beyond the peak, is largely a fingerprint for the electronic properties, including the oxidation state and site symmetry of the absorbing atom. In the EXAFS region the oscillations, which started about ~30 eV beyond the peak of the absorption edge and persisted for another 1000 eV, encoded most of the local structure parameters. ATHENA package codes are used in removing the background contribution to extract EXAFS oscillations. The R-space results displayed in Fig. 2(b) represent the Fourier-transformed spectra derived from the **k**-space data. Clearly, the observed signal [cf. Fig. 2(b)] of the nearest-neighbor (NN) "Se-Cd" shell in the Fourier-transformed absorption exhibited no significant change in character over the range of Se composition. The EXAFS results provided the Cd-Se NN bond length, coordination number N [see Fig. 2(c)], binding energy at the edge E_o, and mean-square displacements $\Delta\sigma^2$ (see Table I) as a function of composition x, revealing little change in the NN bond length from its parent binary compound, CdSe. In Sec. IV B we have used a simple but first-principles bond-orbital model to analyze the EXAFS data.

III. THEORETICAL CONSIDERATIONS

Understanding the phonons in II-VI alloys is significantly important for empathizing and controlling their structural and compositional-dependent characteristics. The existing lattice dynamical theories of disordered semiconductors are, however, not sufficiently sophisticated to make accurate predictions. The Green's-function methodology has been used frequently in constructing models to describe dynamical properties of imperfect solids. The advantage of this approach[57–59] is that it can yield spectral functions and impurity modes measured in optical experiments. There are many texts, monographs, and review articles available giving copious details for calculating the phonon characteristics in imperfect materials.[57–59] Here we succinctly described the Green's-function method within the ATM formalism and constructed two response functions, (a) the dielectric susceptibility $\chi_{\alpha\beta}$ and (b) the scattering $i_{\alpha\gamma\beta\lambda}$ tensors, to study composition-dependent phonon spectra of $CdTe_{1-x}Se_x$ alloys. Both $\chi_{\alpha\beta}$ and $i_{\alpha\gamma\beta\lambda}$ depend upon the correlation between displacements of distant pairs of atoms. These quantities can be evaluated numerically by incorporating host (i.e., zb CdSe and CdTe) lattice phonons from a realistic rigid-ion model[60] and defect perturbations[62] to obtain the composition-dependent impurity modes.

A. Optical response function

Theoretical interpretations of the IR reflectivity/absorption data in polar materials require simulation of the linear response function $\tilde{\varepsilon}_{\alpha\beta}(\omega,\vec{q}) = \tilde{\varepsilon}_{\alpha\beta}(\infty) + 4\pi\chi_{\alpha\beta}(\omega)$. In perfect compound semiconductors, as the $\vec{q} = 0$ selection rule of long-wavelength optical phonons is relaxed, the coupling of $\vec{E}(t) = [\lim_{\delta\to 0} = \vec{E}_o \exp(-i\omega + \delta)t]$ with electric dipole moment $\mathcal{M}$ in an imperfect lattice introduces a perturbation $\mathcal{H}_{\rm int}$ $[= -\mathcal{M}\cdot\vec{E}(t)]$. By solving the Schrödinger equation with Hamiltonian $\mathcal{H}(=\mathcal{H}_o + \mathcal{H}_{\rm int})$ one can obtain the expectation value of the electric dipole moment $\langle\mathcal{M}_\alpha\rangle$ expressed in terms of the dielectric susceptibility $\chi(\omega)$ tensor:[57,58]

$$\langle\mathcal{M}_\alpha\rangle = \sum_\beta \chi_{\alpha\beta}(\omega)E_\beta. \quad (1)$$

For the first-order electric dipole moment, the required susceptibility involves a displacement-displacement $\langle\langle u_\beta(l\kappa,t)u_\gamma(l'\kappa')\rangle\rangle$ correlation function, which can readily be calculated by using the imperfect lattice Green's-function matrix elements:

$$\chi_{\alpha\beta}(\omega) = \lim_{\delta\to 0} - \frac{1}{NV}\sum_{l\kappa\alpha}\sum_{l'\kappa'\beta} Z_\alpha(l\kappa)Z_\beta(l'\kappa') \times G_{\alpha\beta}(l\kappa,l'\kappa';\omega + i\delta), \quad (2)$$

where $Z_\alpha(l\kappa)$ is the effective charge of the atom $(\alpha, l\kappa)$, V is the volume of a single cell, and N is the number of cells in the crystal. In writing Eq. (2), we have used the Fourier transformation with respect to time and related the double-time Green's function of the displacement operators to a classical function as[57]

$$G_{\alpha\beta}(l\kappa,l'\kappa';\omega) = \frac{1}{\hbar}\int_{-\infty}^{\infty} \langle\langle u_\alpha(l\kappa,t)u_\beta(l'\kappa')\rangle\rangle \exp(i\omega t)dt. \tag{3}$$

The above Green's function of the imperfect crystal's Hamiltonian $\mathcal{H}$ satisfies the equation of motion (in matrix notation):

$$\overleftrightarrow{G}^{-1}(\omega) = \overleftrightarrow{M}\omega^2 - \overleftrightarrow{\Phi}, \tag{4}$$

and a similar equation $[\overleftrightarrow{G}_o^{-1}(\omega) = \overleftrightarrow{M}_o\omega^2 - \overleftrightarrow{\Phi}_o]$ exists for the perfect crystal of Hamiltonian $\mathcal{H}_o$. The terms $\overleftrightarrow{M}$ $[\equiv (\overleftrightarrow{M}_o + \Delta\overleftrightarrow{M})]$ and $\overleftrightarrow{\Phi}$ $[\equiv (\overleftrightarrow{\Phi}_o + \Delta\overleftrightarrow{\Phi})]$ in Eq. (4) are, respectively, the mass and force-constant matrices in the "impurity-host" configuration. The well-known Dyson equation relating $\overleftrightarrow{G}$ and $\overleftrightarrow{G}_o$,

$$\overleftrightarrow{G}(\omega) = \overleftrightarrow{G}_o(\omega) + \overleftrightarrow{G}_o(\omega)\overleftrightarrow{P}^i(\omega)\overleftrightarrow{G}(\omega), \tag{5}$$

can be easily iterated to give

$$\overleftrightarrow{G}(\omega) = \overleftrightarrow{G}_o(\omega) + \overleftrightarrow{G}_o(\omega)\overleftrightarrow{P}^i(\omega)\overleftrightarrow{G}_o(\omega) + \overleftrightarrow{G}_o(\omega)\overleftrightarrow{P}^i(\omega)\overleftrightarrow{G}_o(\omega)\overleftrightarrow{P}^i(\omega)\overleftrightarrow{G}_o(\omega)) + \cdots. \tag{6}$$

It is convenient to introduce the $\overleftrightarrow{t}$ matrix to write the expansion in Eq. (6) as

$$\overleftrightarrow{G}(\omega) = \overleftrightarrow{G}_o(\omega) + \overleftrightarrow{G}_o(\omega)\overleftrightarrow{t}^i(\omega)\overleftrightarrow{G}_o(\omega), \tag{7}$$

where

$$\overleftrightarrow{t}^i(\omega) = \overleftrightarrow{P}^i(\omega)[\overleftrightarrow{G} - \overleftrightarrow{I}_o^i(\omega)\overleftrightarrow{P}^i(\omega)]^{-1}. \tag{8}$$

In Eq. (8) we restricted the elements of a perfect lattice Green's function to those sites about i where the elements of $\overleftrightarrow{P}^i$ are nonzero. If $\overleftrightarrow{P}^i$ is large enough, corresponding to a light isolated impurity atom (e.g., CdSe:Mg, CdSe:S) or, for heavier impurity, occupying the lighter host atom (e.g., CdSe:Te), then there will be poles of $\overleftrightarrow{t}^i$ corresponding to the zeros of[62]

$$\mathrm{Re}\{\det(\overleftrightarrow{I} - \overleftrightarrow{G}_o^i\overleftrightarrow{P}^i)\} = 0, \tag{9}$$

causing localized (or gap) mode frequencies above the host lattice (or between the acoustic optical phonon gap) spectrum. On the other hand, for a heavier impurity atom occupying the heavier host atom or for a weak impurity host coupling, one would expect a lower-frequency mode in $\overleftrightarrow{t}^i$ corresponding to the in-band/resonance vibrational feature appearing within the host lattice spectrum. For a pair of defects at sites i and i' the solution of $\overleftrightarrow{t}^{ii'}$ can be carried out exactly with similar results.

B. Self-energy in disordered ternary alloys

To treat the vibrational behavior in ternary $AB_{1-x}C_x$ alloys with finite composition x, we followed the standard treatment of a many-body effect by using the Dyson equation and defined the self-energy for each mode.[57,58] To carry out averaging of the Green's functions over all possible impurity-host configurations, subject to the restriction that impurity concentration x is a fixed quantity, we define

$$\langle\overleftrightarrow{G}\rangle^{-1} = \overleftrightarrow{G}_o^{-1} + \overleftrightarrow{\Sigma}, \tag{10}$$

where the self-energy term $\overleftrightarrow{\Sigma}$ plays the role of an effective perturbation. It can be related in terms of the average $\overleftrightarrow{T}$ matrix by

$$\overleftrightarrow{\Sigma} = [\overleftrightarrow{I} + \langle\overleftrightarrow{T}\rangle\overleftrightarrow{G}_o]^{-1}\langle\overleftrightarrow{T}\rangle. \tag{11}$$

In a multiple-scattering approach $\langle\overleftrightarrow{T}\rangle = \sum_j \langle\overleftrightarrow{T}_j\rangle$, and

$$\begin{aligned}\langle\overleftrightarrow{T}_j\rangle &= \left\langle\left(\overleftrightarrow{I} + \sum_{j'\neq j}\overleftrightarrow{T}_{j'}\overleftrightarrow{G}_o\right)\overleftrightarrow{t}_j\right\rangle \\ &= \left[\overleftrightarrow{I} + \sum_{j'\neq j}\langle\overleftrightarrow{T}_{j'}\rangle\overleftrightarrow{G}_o\right]\langle\overleftrightarrow{t}_j\rangle \\ &\quad + \left\langle\sum_{j'\neq j}(\overleftrightarrow{T}_j - \langle\overleftrightarrow{T}_{j'}\rangle)(\overleftrightarrow{t}_j - \langle\overleftrightarrow{t}_{j'}\rangle)\right\rangle,\end{aligned} \tag{12}$$

where

$$\overleftrightarrow{t}_j = \overleftrightarrow{P}_j(\overleftrightarrow{I} - \overleftrightarrow{G}_o\overleftrightarrow{P}_j)^{-1} \tag{13}$$

describes single-site scattering at the jth impurity of the phonon wave scattered by other impurity atoms. In Eq. (12) the first term represents the scattering of an average incident wave by an atom with an average t matrix. The second term takes into account the correlation between fluctuations in the incident wave and in the atomic $\overleftrightarrow{t}$ matrix. In a single-site approximation one can neglect the correlation term, thus further simplifying $\overleftrightarrow{\Sigma}$ to the following form:

$$\overleftrightarrow{\Sigma} = \sum_j \langle\overleftrightarrow{t}_j\rangle[\overleftrightarrow{I} + \overleftrightarrow{G}_o\langle\overleftrightarrow{t}_j\rangle]^{-1}. \tag{14}$$

It should be mentioned here that the above relations hold even if $\overleftrightarrow{G}_o$ represents the Green's function of an arbitrary reference crystal. For the $CdTe_{1-x}Se_x$ the standard choice in the ATM formalism is to treat the nonrandom alloy as a periodic lattice with anion masses equal to the weighted average between Se and Te atoms. In this case $\overleftrightarrow{\Sigma}$ is exact at both limits of the composition range if the first-order expansion in the defect concentration is carried out. By using the relationship between the dielectric constant and the susceptibility one may obtain $\tilde{\varepsilon}_{\alpha\beta}(\omega)$ in the spectral region of interest and hence the optical phonon properties of alloys.

C. Phonon-assisted Raman scattering in disordered ternary alloys

The relationship between the intensities of the incident and scattered electromagnetic fields is fully exhibited by the fourth-order frequency-dependent scattering $i_{\alpha\gamma\beta\lambda}$ tensor as

$$i_{\alpha\gamma\beta\lambda}(\omega_s) = (2\pi)^{-1}\int_{-\infty}^{\infty} dt\exp(-i\omega_s t)\langle P_{\beta\lambda}(t)P^*_{\alpha\gamma}(0)\rangle, \tag{15}$$

where $\omega_s = \omega_i + \omega$, $P_{\beta\lambda}(t)$ is the time-dependent operator for the electronic polarizability tensor of the crystal, and $\langle\,\rangle$ denotes the thermal average at absolute temperature T. For mixed alloys in the ATM formalism the description of impurity-induced first-order linearly polarized Raman intensity for the unit solid angle Ω and for unit frequency shift ω_s

TABLE II. Optimized set of rigid-ion-model parameters (10^5 dyn/cm; Ref. 60) for studying the lattice dynamics of CdTe and zb CdSe.

Model parameters[a]	CdTe	CdSe
A	−0.1997	−0.24508
B	−0.194	−0.265
C_1	−0.018	−0.024
C_2	−0.017	−0.0295
D_1	−0.0139	0.00725
D_2	−0.0230	−0.041
E_1	0.030	0.0486
E_2	0.040	0.054
F_1	−0.052	−0.0512
F_2	0.072	0.0804
$Z_{\rm eff}$	0.867	0.909
$a_{\rm o}$	6.48 Å	6.077 Å
M_1	112.41 amu	78.96 amu
M_2	127.6 amu	112.41 amu

[a]In the notations of Ref. 60 and $M_1 < M_2$.

$(=\omega_{\rm i} + \omega)$ is given by

$$I(\omega_{\rm i},\omega_{\rm s}:\Omega) \approx \frac{\hbar\omega_{\rm i}^4}{2\pi^2 c^3} \sum_{\alpha\beta\gamma} \sum_{\alpha'\beta'\gamma'} \sum_{l\kappa l'\kappa'} n_\alpha n_{\alpha'} E_\beta E^*_{\beta'} \times \langle P_{\alpha\beta,\gamma}(l\kappa) P_{\alpha'\beta',\gamma'}(l'\kappa')_{\lim\delta\to 0} \times {\rm Im}\langle l\kappa\gamma|\overleftrightarrow{G}(\omega + i\delta)|l'\kappa'\gamma'\rangle\rangle, \quad (16)$$

where n is the thermal occupation number, c is the speed of light, and E_β and $E^*_{\beta'}$ are, respectively, the directions of the electric fields for the incoming and outgoing photons. In Eq. (16), the polarizability tensor due to lattice vibrations is expanded as a function of ionic displacements $\boldsymbol{u}$ and only the terms $\mathcal{P}_{\alpha\beta,\gamma}(l\kappa)$ describing first-order Raman scattering are retained.

IV. NUMERICAL COMPUTATIONS AND RESULTS

Lattice dynamics of II-VI compound semiconductors reflects the specific features about structures and interatomic forces that bind atoms together in the form of a crystal lattice. The simulations of phonons also provides valuable information regarding materials' thermodynamical and defect properties.[59] To comprehend the impurity modes in ternary alloys using ATM–Green's-function theory one needs to evaluate the Green's-function matrix elements[62] and the self-energy terms by incorporating phonons (eigenvalues and eigenvectors) of the host crystals (i.e., CdTe, zb CdSe) from a reliable lattice dynamical scheme.

A. Lattice dynamics of Cd-Zn chalcogenides

Here we have adopted a second-nearest-neighbor rigid-ion model[60] and evaluated the interatomic interactions of CdTe by fitting the inelastic neutron-scattering[37] data. For zb CdSe, the available first-principles results[61,63–66] of the elastic constants, bulk modulus, and critical-point phonons were valuable to us in constructing an optimized model (cf. Table II). The RIM

TABLE III. Comparison of the calculated phonon frequencies (in wave numbers) at the high-symmetry critical points and Debye temperatures (in K) with the existing experimental and theoretical data for CdTe and zb CdSe.

Material	CdTe		CdSe	
properties	Others	Ours	Others	Ours
LO(Γ)	169.3[a]	169.6	218[c], 208[d]	215
TO(Γ)	140[a]	140.2	178[c], 187[d]	178
LO(X)		134.5	190[c], 192[d]	179.7
TO(X)	148[a]	149.9	197[c], 211[d]	194.1
LA(X)		125.3	155[c], 160[d]	155.4
TA(X)	35[a]	35.4	48[c], 53[d]	47.7
LO(L)	144.3[a]	147.8	194[c], 204[d]	184.0
TO(L)	144[a]	142.8	188[c], 204[d]	187.7
LA(L)	108.3[a]	116.2	137[c], 139[d]	148.1
TA(L)	29.3[a]	30.3	34[c], 42[d]	39.3
$\Theta_{\rm D}$ (min)	115[b]	112.6		141.7
$\Theta_{\rm D}$ ($T \to 0$)		170.0	201, 237[e]	223

[a]Reference 37.
[b]Reference 38.
[c]Reference 61.
[d]Reference 64.
[e]Reference 63.

phonon dispersions for CdTe displayed in Fig. 3 are found to be in very good agreement with the experimental data.[37] Theoretical phonon values of the zb CdSe, however, deserved special comments. In its most common phase, CdSe exhibits in the wz crystal structure, whose parameters are almost ideally tetrahedral. In this respect the measured zone-center LO(Γ) 209–211 $\rm cm^{-1}$, TO(Γ) 166–175 $\rm cm^{-1}$ phonons for the wz CdSe are in good agreement with the RIM values of LO(Γ) 215 $\rm cm^{-1}$ and TO(Γ) 178 $\rm cm^{-1}$ phonons for the zb CdSe. Moreover, the calculated phonons at high-symmetry points listed in Table III compared reasonably well with the *ab initio* results of Dal Corso *et al.*[61] By using the standard procedures we have computed [Figs. 3(a) and 3(b)] the one-phonon density of states (DOS), Debye temperatures $\Theta_{\rm D}(T)$, and lattice heat capacities $C_{\rm v}(T)$ [see Figs. 4(a) and 4(b)]. The RIM results of the critical-point phonon energies, $\Theta_{\rm D}(T)$ and $C_{\rm v}(T)$ reported in Table III for CdTe and zb CdSe are compared with the limited experimental or theoretical data.[61,63–66] Due to a small mass difference between Cd (112.4 amu) and Te (127.6 amu) atoms we have noticed a tiny gap in the calculated DOS between acoustical and optical phonon branches of CdTe (126–135 $\rm cm^{-1}$). As the mass difference increased between Cd (112.4 amu) and Se (78.96 amu) atoms, a larger phonon gap was identified from the DOS of zb CdSe (154–178 $\rm cm^{-1}$). These results played important roles relating the specific features of defects responsible for the observed impurity modes in Cd chalcogenides.

B. EXAFS data analysis of $CdTe_{1-x}Se_x$

The bond lengths associated with different chemical species substituted for the cation or anion sublattice sites in II-VI alloys are expected to yield considerable displacements, leading to the relaxations of atoms compared to their original positions in pure compounds. The virtual crystal approximation, which

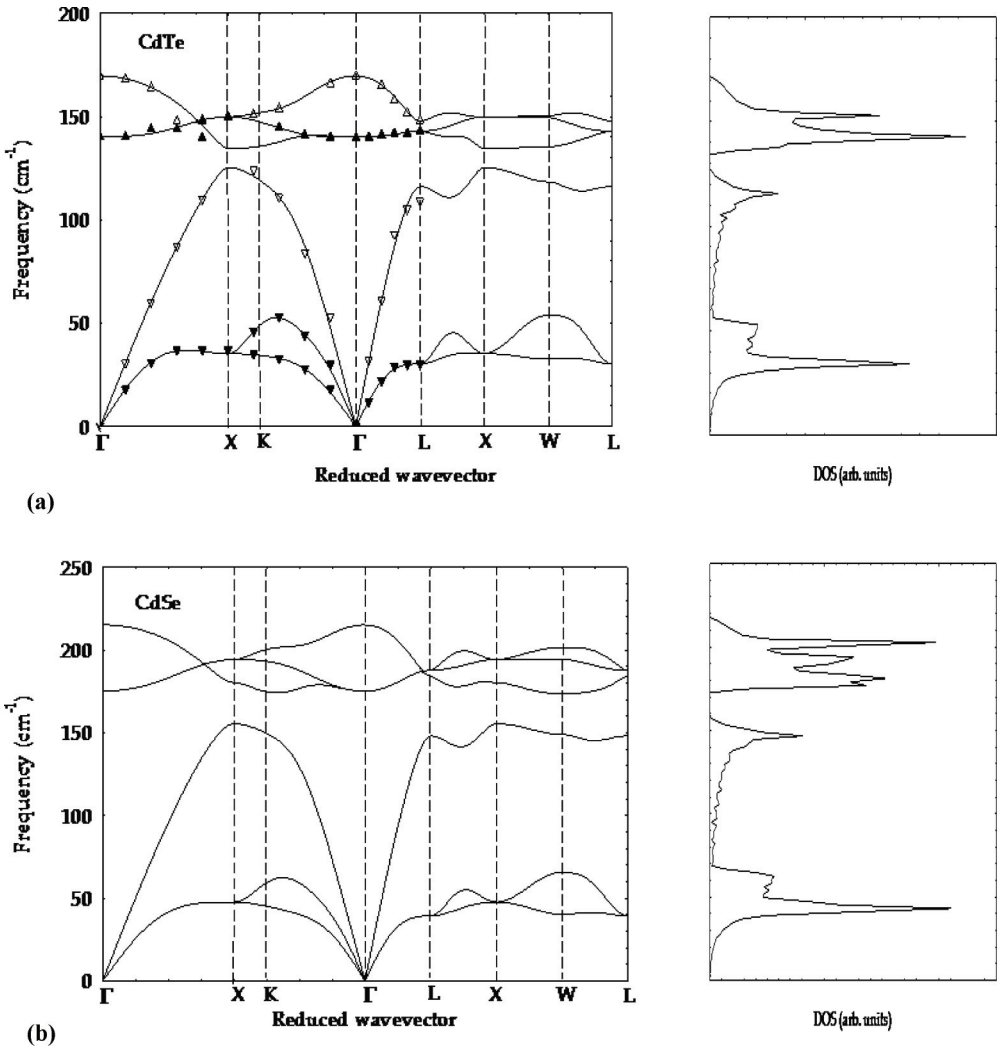

FIG. 3. (left) Comparison of the rigid-ion model calculations (solid line) with the experimental data (open and solid triangles) of the phonon dispersions along the high-symmetry direction and (right) one-phonon density of states using parameter values from Table II for (a) CdTe and (b) zb CdSe.

assumes the bond lengths follow an average value of the binary materials, is proven inappropriate. On the other hand, the EXAFS study has allowed measurements of the local structures in $CdTe_{1-x}Se_x$ alloys with higher accuracy, suggesting that the individual Cd-Te, Cd-Se bond lengths maintained values closer to their parent binary compounds. By using the first-principles BOM,[54–56] we have analyzed the EXAFS data for $CdTe_{1-x}Se_x$ alloys. The calculated total bond energy minimum is used to estimate the lattice distortions and hence the change in bond lengths for the Se/Te substituents in CdTe/CdSe lattice. For $CdTe_{1-x}Se_x$, the x-dependent EXAFS results of the NN bond lengths displayed in Fig. 5 are compared with the BOM and XRD data.[67] Clearly, the analyses of experimental results insinuated much smaller composition-dependent changes in the bond lengths of Cd-Te and Cd-Se than the global average bond length (see Table I) from XRD.[67] The distributions of anion-cation bond lengths are found to be bimodal, and their values as a function of x are closer to those of the reference binary compounds than to the average distance measured by XRD.

C. Impurity modes in Cd-Zn chalcogenides

In Cd chalcogenides, the substitutional defects occupying cation and/or anion sites are expected to give rise to either one or two nonpropagating optically active (infrared/Raman) impurity modes.[68–73] The isolated impurities of light mass replacing lighter host atoms can trigger triply degenerate LVMs at frequencies higher than the maximum phonon (ω_m) frequency of the perfect lattice.[68] On the other hand, a light impurity occupying the heavier host atom can give rise to both a high-frequency LVM and a gap mode (falling between the gaps of acoustic and optical bands of the host lattice phonons, e.g., GaP:B).[68] In the binary zb CdSe, it is possible for the gap mode to occur for heavier Te impurities occupying the lighter Se (Te_{Se}) host atoms.[62,69]

To comprehend the vibrational properties of defects in CdTe or zb CdSe compounds we have adopted the ATM–Green's-function theory (cf. Sec. II B). To make the computational aspects of the problem manageable, reasonable assumptions are made (see Ref. 62) in defining the perturbation $\overleftrightarrow{P}^i$ to keep the defect subspace as small as possible. The Green's

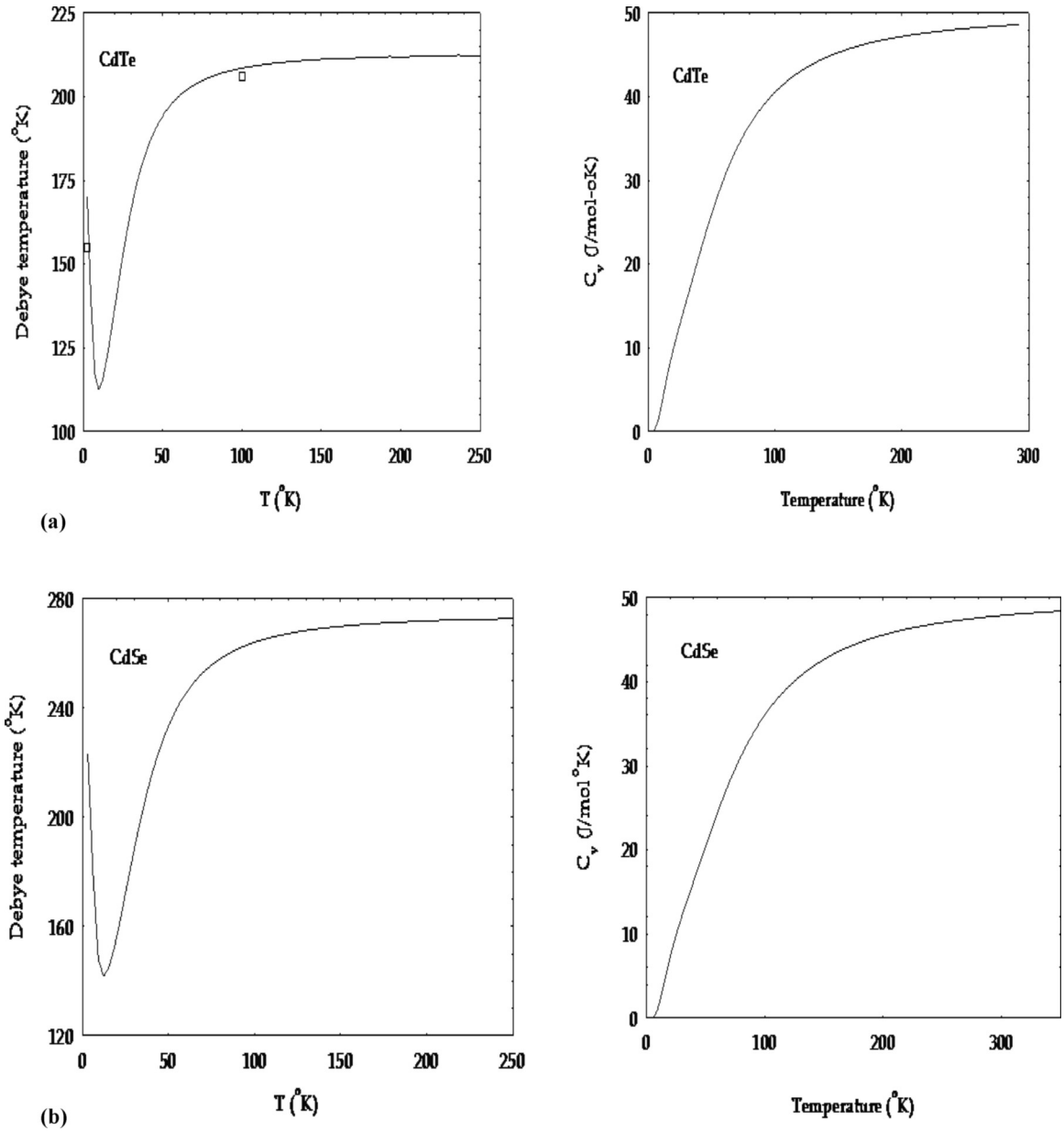

FIG. 4. (left) Comparison of the rigid-ion model calculations (solid line) with the experimental data (squares) of the Debye temperature Θ_D(T) and (right) specific heat $C_v(T)$ using parameter values from Table II for (a) CdTe and (b) zb CdSe.

functions for the imperfect systems are evaluated numerically using a root-sampling technique by incorporating the host lattice phonons at 64 000 $\vec{q}$ points in the Brillouin zone. To assess the validity of our approach, we have displayed in Figs. 6(a) and 6(b) the calculated triply degenerate F_2 LVMs for several light isolated impurity atoms (T_d symmetry) occupying the Cd or Se sites in zb CdSe as a function of radial force-constant change parameter t or u. The implications of impurity perturbation parameters (t and u) for the two different I_{Cd} and I_{Se} configurations are described in detail elsewhere.[62] A comparison of the calculated LVM modes[62] for isolated light S_{Se}, O_{Se} [cf. Fig. 6(b)] defects in zb CdSe has provided a very good agreement with the experimental and first-principles data.[73] As expected, Figs. 6(a) and 6(b) have clearly shown the decrease of LVM frequencies with the increase of impurity mass M_i^I (with $i \equiv$ Cd and Se). One must note that the LVM frequency can fall within the band continuum if defect mass becomes heavier than a critical value.

D. Phonon modes in $CdTe_{1-x}Se_x$ alloys

The vibrational characteristics in $AB_{1-x}C_x$ ternary alloys, depending upon the constituent atomic masses A, B, and C, can exhibit a variety of interesting phenomena, including the so-called one-mode, two-mode, and intermediate mixed-mode behaviors. Based on Chang-Mitra's (CM) effective mass (μ_{AC}, μ_{AB}) approach,[51] many efforts have been expended within the MREI methodology to predict *a priori* the expected types of phonon-mode behaviors in ternary compounds.[39] It is worth mentioning, however, that the CM-MREI scheme[51] cannot

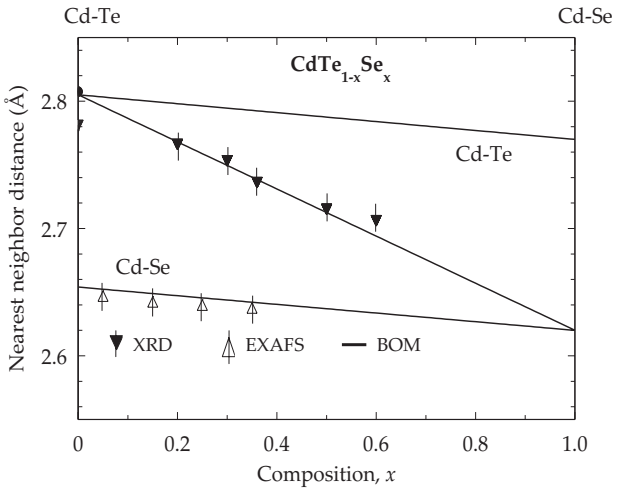

FIG. 5. Comparison of EXAFS data (open triangles) with the BOM calculation for the distribution of nearest-neighbor anion-cation distances in $CdSe_xTe_{1-x}$ ternary alloys as a function of x. X-ray data (solid triangles) of the average bond length (see Ref. 68) for the cubic phase of $CdTe_{1-x}Se_x$ ternary alloys and of CdTe (dot) are also reported.

account for the changes observed in IR reflectivity/Raman line shapes in several borderline cases (i.e., intermediate and two-mode behavior), including the one represented here (i.e., $CdSe_xTe_{1-x}$; see Ref. 39). The simple reason is that in the CM-MREI approach one assumes (a) an ideal effective homogeneous medium at the local region while the statistical average of neighboring atoms depends upon the composition x and (b) the anions and cations of like species vibrate with the same phase and amplitude while the force experienced by each ion is conferred by the statistical average of interactions with its neighbors.

Before presenting our ATM–Green's-function results on impurity modes in $CdSe_xTe_{1-x}$, we must note that the Raman and/or IR reflectivity studies have indicated no overlap of the long-wavelength optical [LO(Γ) – TO(Γ)] phonons in the binary zb CdTe,[37] CdSe materials.[61–64] This is one of the basic criteria for the ternary alloy to exhibit a two-mode-behavior.[51] In order to comprehend the vibrational characteristics in $CdSe_xTe_{1-x}$ using ATM–Green's-function theory we have focused our inquisition near the extreme composition limits where most of the Se or Te atoms are isolated in the CdTe-like or CdSe-like matrix. The analyses of EXAFS data for the NN

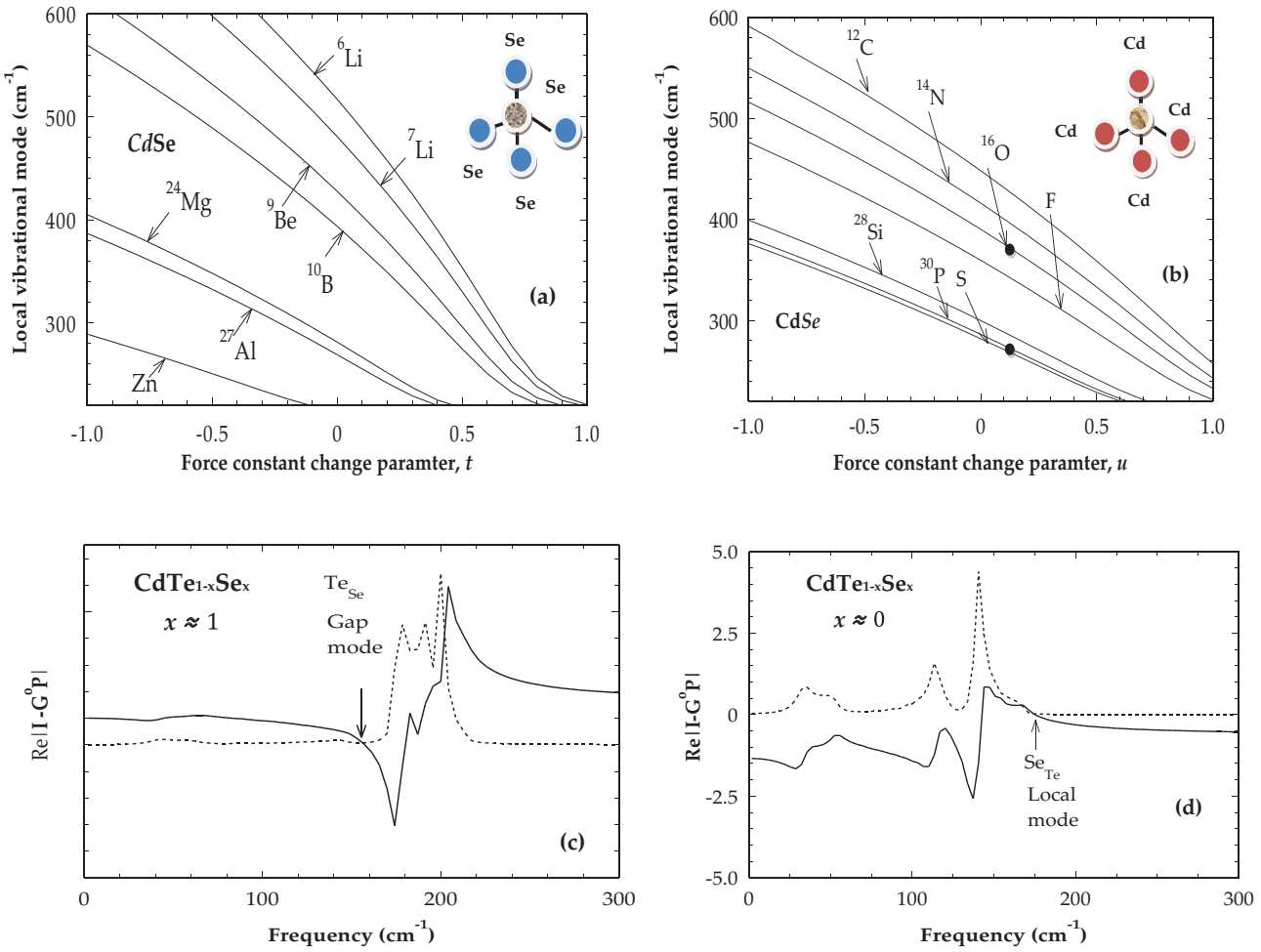

FIG. 6. (Color online) Calculated F_2 localized vibrational modes in CdSe data for defects (a) occupying the Cd site vs the force-constant change parameter t and (b) occupying the Se site vs the force-constant change parameter u; experimental results are represented by dots. (c) The graphical solution of Eq. (9) for $CdSe_xTe_{1-x}$ ternary alloys (see text) near $x \approx 1$, predicting the gap mode of Te_{Se} near ∼157 cm^{-1}, and (d) a localized vibrational mode for $x \approx 0$ Se_{Te} near ∼174 cm^{-1}.

bond lengths around Se/Te atoms in the CdTe/CdSe matrix using a first-principles BOM enabled us to estimate the lattice relaxations affecting the necessary force constants.[54–56] The values of radial force constants at impurity sites required for defining the perturbations are obtained from the second derivatives of the bond energies.[54–56] Based on the BOM we have determined appropriate force-constant variations for Se_{Te} (i.e., of Cd-Se bond) defects in the CdTe matrix and for the Te_{Se} (i.e., of Cd-Te bond) impurities in the CdSe matrix. Numerical simulations of the self-energy terms to the lowest/highest order of x are carried out to appraise the composition-dependent phonon features in $CdSe_xTe_{1-x}$.

The graphical solutions of Eq. (9) for the $CdSe_xTe_{1-x}$ alloys in the two extreme composition limits are displayed [see Figs. 6(c) and 6(d)] in the frequency range of 0–300 cm^{-1}. The dotted lines in Figs. 6(c) and 6(d) represent the spectral density of states, while the solid lines symbolize the real part of Eq. (9). The frequencies of the gap and LVMs are identified in the two alloy systems by the poles (i.e., the crossing of the real part) of Eq. (9) through zeros in the region of low DOS. In agreement with the experimental results[52] our study for $x \approx 1$ provided a clear revelation of the gap mode at $\sim$157 cm^{-1} [Fig. 6(c)] for the heavier Te atoms occupying Se sites and of the local mode at $\sim$174 cm^{-1} [Fig. 6(d)] due to the lighter Se atoms on Te sites for $x \approx 0$. Surprisingly, the calculated LVM of Se_{Te} in the limiting case $x \to 0$ falls close to the frequency of an unresolved phonon line observed in the low-temperature IR reflectivity measurements.[43,52] Again, the numerically simulated value for the gap mode of Te_{Se} in the extreme situation $x \to 1$ lies well between the gap of the acoustic and optical modes of CdSe, in good agreement with experimental data. In the ternary $CdSe_xTe_{1-x}$ alloy this signifies that the CdTe zone-center optical modes at $x = 0$ converge to the gap mode of Te_{Se} in CdSe at $x \approx 1$. Similarly, the CdSe optical phonons at $x = 1$ congregate to the local mode of Se_{Te} in CdTe as x approaches zero (i.e., $x \approx 0$). Again at $x \approx 1$, the Te_{Se} gap mode in CdSe has a lower frequency than the two zone-center optical modes of CdSe appearing well within the gap between the optical and acoustical phonons, whereas at $x \approx 0$, the Se_{Te} local mode in CdTe has a slightly higher frequency than the two zone-center optical modes of CdTe. Clearly, the ATM–Green's-function results have strongly substantiated our experimental observations of the two-phonon-mode behavior for the $CdSe_xTe_{1-x}$ alloys.[52]

V. SUMMARY AND CONCLUSIONS

Comprehensive measurements of the optical and structural properties of $CdSe_xTe_{1-x}$ alloys ($0.35 \geqslant x \geqslant 0.05$) grown by using the Bridgman technique are reported using Raman scattering and EXAFS spectroscopy, respectively. While the Raman spectroscopy provided results for the optical phonon modes in $CdSe_xTe_{1-x}$, the EXAFS measurements performed on the same material samples revealed valuable data on the composition-dependent nearest-neighbor bond lengths d, coordination number N, binding energy at the edge E_o, and mean-square displacements $\Delta\sigma^2$. For the ternary $CdSe_xTe_{1-x}$ alloys, the comparison of Raman spectra with IR reflectivity[43,52] data in the long-wavelength region has undoubtedly exposed two major phonon modes in the energy range of 140–200 cm^{-1}. In the alloy zb structure, while the IR phonon spectra is primarily modulated by the TO modes, these phonons in the (100) backscattering configuration of the Raman spectroscopy are either forbidden or hardly conspicuous. In the $CdSe_xTe_{1-x}$ alloys with $x \geqslant 0.05$, it is the IR reflectivity[43,52] that provided indications of the splitting of a CdSe-like TO mode at $\sim$180 cm^{-1} into an additional weak phonon feature appearing on the lower-energy side near $\sim$175 cm^{-1}. Although Perkowitz *et al.*[43] interpreted the extra mode originating from the nonrandom substitutions of the negative ions clustering around the positive ions, the weak feature was contemplated as a LVM of Se_{Te} in CdTe. Detailed analyses of the EXAFS data using a first-principles[54–56] BOM have enabled us to estimate the bond length relaxations and NN radial force constants around the Se/Te atoms in the CdTe/CdSe matrix. This crucial information is methodically integrated into the ATM–Green's-function theory in defining the defect perturbations to comprehend the composition-dependent optical phonons in $CdTe_{1-x}Se_x$ alloys. Our calculations of impurity modes in the low-composition regime, i.e., $x \to 0$, have substantiated an earlier assertion that the weak phonon feature observed near $\sim$175 cm^{-1} in the low-temperature IR reflectivity experiments is related to the Se_{Te} localized vibrational mode. Additional polarization-dependent IR reflectivity and Raman scattering studies of several II-II-VI and II-VI-VI alloys now underway should further help authenticate our theoretical conjectures to definitive understanding.

ACKNOWLEDGMENTS

D.N.T. acknowledges useful discussions on the subject matter with M. D. Tiwari of the Indian Institute of Information Technology, Allahabad, India, and for the Innovation Grant that he received from the School of Graduate Studies at Indiana University of Pennsylvania, Indiana, Pennsylvania. The work at the National Taiwan University was supported by Grants No. NSC 98-2221-E-002-015-MY3 and No. NSC 98-3114-E-005-002-CC2 and by NTU Excellent Research Projects No. 10R80908 and No. 102R890954.

*talwar@iup.edu
†zcfeng@ntu.edu.tw

[1] S. Adachi, *Properties of Semiconductor Alloys*, Wiley Series in Materials for Electronic and Optoelectronic Applications (Wiley, Hoboken, NJ, 2009).
[2] G. E. Hallani, A. Ryah, N. Hassanain, M. Loghmarti, A. Mzerd, A. Arbaoui, N. Achargui, Y. Laaziz, N. Chahboun, and E. K. Hlil, in *Progress in Electromagnetics Research Symposium Proceedings, Marrakesh, Morocco, March 20–23* (The Electromagnetics Academy, Cambridge, MA, 2011), p. 1897.
[3] T. Park, J. Lee, W. Lee, J. Ahn, and W. Yi, in *22nd Intl. Vacuum Nanoelectronics Conference (IVNC 2009), Shizuoka, July 20–24* (IEEE, Piscataway, NJ, 2009), p. 275.

[4]W. J. Min, J. Sunghan, J. L. Sung, K. Yongwook, and S. S. Koo, J. Phys. Chem A **113**, 9588 (2009).

[5]C. Reig, M.-D. Cubells-Beltrán, and D. Ramírez Muñoz, Sensors **9**, 7919 (2009).

[6]M. B. Reine, Proc. SPIE **7298**, 72982S (2009).

[7]*The Handbook of Photonics*, edited by M. C. Gupta and J. Ballato, 2nd ed. (CRC, New York, 2007).

[8]S. Stepanov, in *Handbook of Advanced Electronic and Photonic Materials and Devices*, edited by H. S. Nalwa (Academic Press, San Diego, 2001), Vol. 2, p. 205.

[9]*II-VI Semiconductor Materials and their Applications*, edited by M. C. Tamargo, Optoelectronic Properties of Semiconductors and Superlattices Vol. 12 (Taylor and Francis, New York, 2001).

[10] *Opto-electronic Applications*, edited by H. Ruda (Chapman & Hall, London, 1992), p. 415.

[11]H. Qiao, B. Guan, T. Böcking, M. Gal, J. J. Gooding, and P. J. Reece, Appl. Phys. Lett. **96**, 161106 (2010).

[12]C. Reig, C. Gómez-García, and S. V. Muñoz, J. Microelectron. **38**, 327 (2007).

[13]I. L. Medintz, H. T. Uyeda, E. R. Goldman, and H. Mattoussi, Nat. Mater. **4**, 435 (2005).

[14]X. Liu and J. K. Furdyna, J. Appl. Phys. **95**, 7754 (2004).

[15]Y. Luo, S. P. Guo, O. Maksimov, M. C. Tamargo, V. Asnin, F. H. Pollak, and Y. C. Chen, Appl. Phys. Lett. **77**, 4259 (2000).

[16]Z. Yu, D. B. Eason, C. Boney, J. Ren, W. C. Hughes, W. H. Rowland, Jr., J. W. Cook, Jr., J. F. Schetzina, G. Cantwell, and W. C. Harsch, J. Vac. Sci. Technol. B **13**, 711 (1995).

[17]L. A. Kolodziejski, R. L. Gunshor, and A. V. Nurmikko, Annu. Rev. Mater. Sci. **25**, 711 (1995).

[18]A. Salokatve, K. Rakennus, P. Uusimaa, M. Pessa, T. Aherne, J. P. Doran, J. O'Gorman, and J. Hegarty, Appl. Phys. Lett. **67**, 407 (1995).

[19]S. Permogorov and A. Reznitsky, J. Lumin. **52**, 201 (1992).

[20]A. Tu and P. D. Persans, Appl. Phys. Lett. **58**, 1506 (1991).

[21]P. Kuznetsov, V. Lusanov, G. Yakushcheva, V. Jitov, L. Zakharov, I. Kotelyanskii, and V. Kozlovsky, Phys. Status Solidi C **7**, 1568 (2010).

[22]M. M. Zverev, D. V. Peregudov, I. V. Sedova, S. V. Sorokin, S. V. Ivanov, and P. S. Kop'ev, Quantum Electron. **34**, 909 (2004).

[23]O. de Melo, C. Vargas, and I. Hernandez-Calderon, Appl. Phys. Lett. **82**, 43 (2003).

[24]J. Huerta, M. López, and O. Zelaya, Superficies Vacio **8**, 125 (1999).

[25]L. C. Calhoun and R. M. Park, J. Appl. Phys. **85**, 490 (1999).

[26]F. Gindele, U. Woggon, W. Langbein, J. M. Hvam, K. Leonardi, D. Hommel, and H. Selke, Phys. Rev. B **60**, 8773 (1999).

[27]L. Worschech, W. Ossau, W. Behr, Th. J. Nurnberger, and G. Landwehr, Appl. Phys. Lett. **73**, 835 (1998).

[28]S. V. Ivanov, A. A. Toropov, S. V. Sorokin, T. V. Shubina, N. D. Il'inskaya, A. V. Lebedev, I. V. Sedova, P. S. Kop'ev, Zh. I. Alferov, H.-J. Lugauer, G. Reuscher, M. Keim, F. Fischer, A. Waag, and G. Landwehr, Semiconductors **32**, 1137 (1998).

[29]L. H. Kuo, L. Salamanca-Riba, B. J. Wu, G. M. Haugen, J. M. DePuydt, G. Hofler, and H. Cheng, J. Vac. Sci. Technol. B **13**, 1694 (1995).

[30]M. Hetterich, M. Grün, H. Gerlach, and C. Klingshirn, Mater. Sci. Forum **182-184**, 415 (1995).

[31]W. Shan, S. J. Hwang, J. M. Hays, J. J. Song, Z. Q. Zhu, and T. Yao, J. Appl. Phys. **74**, 5699 (1993).

[32]H. Jeon, J. Ding, A. V. Nurmikko, W. Xie, D. C. Grillo, M. Kobayashi, R. L. Gunshor, G. C. Hua, and N. Otsuka, Appl. Phys. Lett. **60**, 2045 (1992).

[33]N. Samarth, H. Lou, J. K. Furdyna, S. B. Qadri, Y. R. Lee, A. K. Ramdas, and N. Otsuka, Appl. Phys. Lett. **54**, 2680 (1989); O. de Melo, E. Sanchez, H. Rodriguez, S. de Roux, F. Rabago-Bernal, and J. Rouiz-Garcia, Mater. Chem. Phys. **59**, 120 (1999); K. Ichino, Y.-H. Wu, Y. Kawakami, S. Fujita, and S. Fujita, J. Cryst. Growth **117**, 527 (1992).

[34]E. Deligoz, K. Colakoglu, and Y. Ciftci, Phys. B **373**, 124 (2006).

[35]M. Gaith and I. Alhayek, Rev. Adv. Mater. Sci. **21**, 183 (2009).

[36]S. Ouendadji, S. Ghemid, H. Meradji, and E. El Haj Hassan, Comput. Mater. Sci. **50**, 1460 (2011).

[37]J. M. Rowe, R. M. Nicklow, D. L. Price, and K. Zanio, Phys. Rev. B **10**, 671 (1974); N. Vagelatos, D. Wehe, and J. S. King, J Chem. Phys. **60**, 3613 (1974).

[38]T. H. K. Barron, J. G. Collins, and G. K. White, Adv. Phys. **29**, 609 (1980); T. H. K. Barron, J. A. Birch, and G. K. White, J. Phys. C **10**, 1817 (1977).

[39]S. Jiménez-Sandoval, A. López-Rivera, and J. C. Irwin, Phys. Rev. B **68**, 054303 (2003).

[40]M. Gorska and W. Nazarewicz, Phys. Status Solidi B **57**, K65 (1973); **65**, 193 (1974).

[41]E. A. Vinogradov, L. K. Vodop'yanov, and G. S. Oleinik, Sov. Phys. Solid State **15**, 322 (1973).

[42]V. G. Plotnichenko, L. V. Golubev, and L. K. Vodop'yanov, Sov. Phys. Solid State **19**, 1582 (1977).

[43]S. Perkowitz, L. S. Kim, and P. Becla, Phys. Rev. B **43**, 6598 (1991).

[44]N. Motta, A. Balzarotti, P. Letardi, A. Kisiel, M. T. Czyzyk, M. Zimnal-Starnawska, and M. Podgorny, Solid State Commun. **53**, 509 (1985).

[45]R. A. Mayanovic, W. F. Pong, and B. A. Bunker, Phys. Rev. B **42**, 11174 (1990).

[46]G. J. Camargo-Gamboa, J. S. Lezama Pacheco, J. Mustre de León, S. D. Conradson, and I. Hemández-Calderón, Thin Solid Films **490**, 165 (2005).

[47]W.-F. Pong, Ph.D. thesis, University of Notre Dame, 1989.

[48]B. V. Robouch, A. Kisiel, A. Marcelli, M. Cestelli Guidi, M. Piccinini, E. Burattini, and A. Mycielski, J. Alloys Compd. **426**, 31 (2006).

[49]W.-C. Zheng, S.-Y. Wu, and W. Li, J. Phys. Chem. Solids **61**, 489 (2000).

[50]I. J. Hsu, R. S. Liu, J. M. Chen, R. G. Liu, L. Y. Jang, J. F. Lee, and K. D. M. Harris, Chem. Mater. **12**, 1115 (2000).

[51]I. F. Chang and S. S. Mitra, Phys. Rev. **172**, 924 (1968).

[52]D. N. Talwar, T.-R. Yang, Z. C. Feng, and P. Becla, Phys. Rev. B **84**, 174203 (2011).

[53]H. W. Verleur and A. S. Barker, Phys. Rev. **149**, 715 (1966).

[54]W. A. Harrison, *Electronic Structure and the Properties of Solids* (Freeman, San Francisco, 1980).

[55]D. N. Talwar, K. S. Suh, and C. S. Ting, Philos. Mag. B **56**, 593 (1987).

[56]D. N. Talwar, Z. C. Feng, and P. Becla, Phys. Rev. B **48**, 17064 (1993).

[57]A. A. Maradudin, E. W. Montroll, G. H. Weiss, and I. P. Ipatova, in *Solid State Physics*, 2nd ed., edited by F. Seitz, D. Turnbull, and H. Ehrenreich (Academic, New York, 1971).

[58]R. J. Elliott, J. A. Krumhansl, and P. L. Leath, Rev. Mod. Phys. **46**, 465 (1974); R. Kubo, J. Phys. Soc. Jpn. **12**, 570 (1957).

[59]D. N. Talwar, in *Dilute III-V Nitride Semiconductors and Material Systems: Physics and Technology*, edited by A. Erol, Springer Series in Materials Science Vol. 105 (Springer, Berlin, 2008), Chap. 9, p. 222.
[60]K. Kunc, Ann. Phys. (Paris) **8**, 319 (1973-74).
[61]A. Dal Corso, S. Baroni, R. Resta, and S. de Gironcoli, Phys. Rev. B **47**, 3588 (1993).
[62]D. N. Talwar, Z. C. Feng, and T.-R. Yang, Phys. Rev. B **85**, 195203 (2012).
[63]J. J. Tan, Y. Cheng, W. J. Zhu, and Q. Q. Gou, Commun. Theor. Phys. **50**, 220 (2008).
[64]S. Q. Wang, Mater. Sci. Forum **561**, 1907 (2007).
[65]M. Cotè, O. Zakharov, A. Rubio, and M. L. Cohen, Phys. Rev. B **55**, 13025 (1997).
[66]S. H. Wei and S. B. Zhang, Phys. Rev. B **62**, 6944 (2000).
[67]J. Litwin, Phys. Status Solidi **5**, 551 (1964).
[68]R. C. Newman, in *Semiconductors and Semimetals*, edited by E. Weber (Academic, New York, 1993), Vol. 38, Chap. 4; D. A. Robbie, M. J. L. Sangster, E. G. Grosche, R. C. Newman, T. Pletl, P. Pavone, and D. Strauch, Phys. Rev. B **53**, 9863 (1996).
[69]Y. M. Azhniuk, Y. I. Hutych, V. V. Lopushansky, M. V. Prymak, A. V. Gommonai, and D. R. T. Zahn, Int. J. Spectrosc. **2012**, 495896 (2012).
[70]A. Mujica, A. Rubio, A. Munoz, and R. J. Needs, Rev. Mod. Phys. **75**, 863 (2003).
[71]N. J. Lee, R. K. Kalia, A. Nakano, and P. Vashishta, Appl. Phys. Lett. **89**, 093101 (2006).
[72]O. Pagès, T. Tite, H. Kim, P. A. Graf, O. Maksimov, and M. C. Tamargo, J. Phys. Condens. Matter **18**, 577 (2006).
[73]J. T-Thienprasert, S. Limpijumnong, M.-H. Du, and D. J. Singh, Physica **407**, 2841 (2012).